HHS Public Access

Author manuscript

Nat Immunol. Author manuscript; available in PMC 2016 September 28.

Published in final edited form as:

Nat Immunol. 2016 May ; 17(5): 545–555. doi:10.1038/ni.3408.

Classical dendritic cells are required for dietary antigen-mediated peripheral regulatory T cell and tolerance induction

Daria Esterházy[1], **Jakob Loschko**[2], **Mariya London**[1], **Veronica Jove**[1], **Thiago Y. Oliveira**[2], and **Daniel Mucida**[1]

[1]Laboratory of Mucosal Immunology, The Rockefeller University, New York, NY 10065, USA.

[2]Laboratory of Molecular Immunology, The Rockefeller University, New York, NY 10065, USA.

Abstract

Oral tolerance prevents pathological inflammatory responses towards innocuous foreign antigens via peripheral regulatory T cells (pT_{reg} cells). However, whether a particular subset of antigen-presenting cells (APCs) is required during dietary antigen exposure to instruct naïve $CD4^+$ T cells to differentiate into pT_{reg} cells has not been defined. Using myeloid lineage-specific APC depletion in mice, we found that monocyte-derived APCs are dispensable, while classical dendritic cells (cDCs) are critical for pT_{reg} cell induction and oral tolerance. $CD11b^-$ cDCs from the gut-draining lymph nodes efficiently induced pT_{reg} cells, and conversely, loss of IRF8-dependent $CD11b^-$ cDCs impaired their polarization, although oral tolerance remained intact. These data reveal the hierarchy of cDC subsets in pT_{reg} cell induction and their redundancy during oral tolerance development.

The peripheral immune system must maintain a balance between protective responses and tolerance. This equilibrium represents a major challenge for the mucosal surfaces, particularly the intestine, which is chronically exposed to both potentially pathogenic microbes and harmless dietary and commensal-derived antigens. Not surprisingly, several cellular and molecular mechanisms exist to ensure robust tolerance induction in the mucosae.

Peripherally-induced $Foxp3^+$ regulatory T cells (pT_{reg} cells) are thought to be instrumental in the induction and maintenance of peripheral tolerance[1, 2, 3, 4]. Innocuous antigen exposure

Correspondence should be addressed to D.M. (; Email: mucida@rockefeller.edu), P. 212-327-7520, F. 212-327-8370

Author contributions

D.E. designed the study, performed the experiments unless stated otherwise below and wrote the manuscript; J.L. generated the *zDC-Cre* mice, backcrossed them onto the *Irf8*$^{fl/fl}$ background, carried out their hematopoietic characterization (Fig. 7) and substantially contributed to the design of experiments; M.L. and V.J. significantly contributed to the establishment of oral tolerance protocols and to the oral tolerance experiments; T.O. performed the bioinformatic analysis of the RNA-seq experiments; D.M. initiated, designed and supervised the study, performed experiments and wrote the manuscript.

Accession Codes

All RNA-seq data are submitted to NCBI's Gene Expression Omnibus, with the accession number GEO (pending).

Competing financial interests

The authors declare no competing financial interests.

via mucosal surfaces efficiently induces pT_{reg} cell differentiation from naïve $CD4^+$ T cells via a retinoic acid (RA)- and TGF-β-dependent process[2, 5, 6, 7, 8]. In turn, genetic loss-of-function strategies that target pT_{reg} cells result in severe inflammatory phenotypes in the lungs and intestine [3, 4].

Antigen presenting cells (APCs), including dendritic cells (DCs) and macrophages, have been ascribed critical roles in triggering pT_{reg} cell differentiation[6, 7, 8, 9, 10]. In particular, intestinal APCs expressing the fraktalkine receptor CX3CR1 take up soluble luminal antigens [11, 12] and, under certain conditions, migrate to the mesenteric lymph nodes (mLNs) where they present antigens to naïve T cells[13]. In addition, CX3CR1–expressing phagocytes appear to transfer antigens to neighboring migratory DCs[11] and these DCs are believed to induce pT_{reg} cell conversion after they migrate to the mLNs[14, 15]. Indeed, both lamina propria and mLN-derived DCs, particularly αE integrin$^+$ ($CD103^+$) or $DEC205^+$ DCs, produce high amounts of RA and TGF-β and efficiently induce pT_{reg} cells [1, 6, 7, 8, 16, 17, 18, 19]. However, whether these pT_{reg} cell-inducing APCs are also required for oral tolerance induction has not been investigated. Furthermore, because the strategies relying on cell surface markers utilized to date target multiple APC lineages, the exact nature and origin of APCs responsible for pT_{reg} cell induction *in vivo* are still unclear.

We demonstrate an essential role for pre-DC–derived classical dendritic cells (cDCs) for both pT_{reg} cell and oral tolerance induction, while macrophages and monocyte-derived cells appear dispensable. Further, we identify a hierarchical pattern in pT_{reg} cell-inducing capacity of mLN-derived cDC subsets, whereby dietary antigen mediated pT_{reg} cell polarization is most dependent on migratory IRF8–dependent $CD11b^-$ cDCs. Oral tolerance is intact, however, in absence of this cDC subset, highlighting robustness of the process and functional redundancy of cDCs.

Results

Systemic absence of cDCs leads to break in oral tolerance

We first set out to determine whether the APCs required for induction of oral tolerance could be classified by one of the two major myeloid lineages (**Supplementary Fig. 1a**). We focused on the populations present in the mLNs, the major inductive sites of oral tolerance[14]. Macrophages were identified as $Lin^-MHCII^+CD11c^+CD64^+$ cells, and cDCs as $Lin^-MHCII^+CD11c^+CD64^-$ cells (**Fig. 1a**)[20]. Within the cDCs, we distinguished between two resident $MHCII^{int}$ populations, $CD8\alpha^+CD11b^{low}$ versus $CD8\alpha^-CD11b^+$ and two migratory $MHCII^{hi}$ populations, $CD103^+CD11b^-$ versus $CD103^+CD11b^+$ (**Fig. 1a**). We first used a mouse model of T_H1 delayed-type hypersensitivity (DTH) [9] to address whether a specific APC lineage is required for the induction phase of oral tolerance. Tolerance was assessed by measuring the cellular and humoral inflammatory immune response towards OVA in mice pre-exposed to oral ovalbumin (OVA) or oral PBS as control and immunized with OVA in complete Freund's adjuvant (CFA) (**Fig. 1b**). We targeted the macrophage-monocyte lineage using mice bearing the Cre recombinase gene under the *Lyz2* promoter, and the diphtheria toxin receptor (DTR) gene preceded by a *loxP* site-flanked stop cassette under control of the *Csf1r* promoter ($Lyz2^{Cre} \times Csf1r^{LsL\text{-}DTR}$, herein called MM^{DTR} mice)[20] and the pre-DC-derived lineage using mice with DTR knocked in 3' of the pre-DC lineage

transcription factor *Zbtb46* gene (*Zbtb46*^{DTR}, herein called zDC^{DTR} mice)[21]. Because DT is lethal to zDC^{DTR} mice, due to Zbtb46 expression in vascular endothelium[21], we used chimeric mice in which total bone marrow (BM) cells from zDC^{DTR}, MM^{DTR} or wild-type littermate control mice were transferred into lethally irradiated C57BL/6 mice. Administration of DT to MM^{DTR} mice led to broad depletion of monocytes, monocyte– and yolk sac–derived tissue macrophages and inflammatory DCs, which lasted for at least 36h[20] (**Supplementary Fig. 1b, c**), while DT administration to zDC^{DTR} mice resulted in a compensatory surge of Flt3L (FMS-like tyrosine kinase 3 ligand) in the serum, and complete loss of cDCs, including migratory cDC subsets in the mLN[20] (**Supplementary Fig. 1c, d**). To induce oral tolerance, OVA was gavaged 12 and 30 hours after the first of three DT injections given 36 hours apart, and DT and OVA administration were timed such that OVA clearance (completed after 24 hours) preceded the reappearance of APCs[20] (**Supplementary Fig. 1e-h**). To rule out that DT administration to the bone marrow chimeric mice resulted in altered oral antigen absorption, we measured OVA uptake into different tissues at 4 hours post OVA gavage (**Supplementary Fig. 1i-m**). Because APCs are required for immune responses, mice were immunized with OVA+CFA 8 days after the last DT dose, when the APC niches were replenished (**Fig. 1b** and **Supplementary Fig. 1n, o**), followed by subcutaneously injection with OVA in the ear 14 and 24 days after immunization.

At 72 hours post ear injection, ear swelling, serum anti-OVA IgG1 and anti-OVA IgG2c amounts were suppressed in OVA-fed wild-type and MM^{DTR}, but not in zDC^{DTR} mice, when compared to their PBS-fed counterparts **(Fig. 1c-e)**. We noticed that PBS-fed, OVA-CFA immunized zDC^{DTR} mice produced reduced serum IgG amounts compared to wild-type or MM^{DTR} mice, likely a consequence of the overall reduced CD4^{+} T cell frequency upon recent cDC depletion (**Supplementary Fig. 1o**). As a positive control for the APC-dependence of oral tolerance induction, we also studied chimeric mice lacking all CD11c-expressing APCs[20, 22] by using BM from mice expressing DTR under control of the *Itgax* promoter, the gene encoding integrin CD11c (here CD11c^{DTR} mice)[20, 22]. PBS-fed and OVA-fed CD11c^{DTR} mice showed similar ear swelling and serum anti-OVA antibody responses (**Fig. 1c-e**), suggesting lack of tolerance to OVA. These observations indicated that monocyte-macrophage–derived APCs are dispensable for oral tolerance induction, while pre-DC–derived cells are critical.

Next, we assessed the requirement for cDCs in preventing T_H2 allergic responses[2] (**Fig. 2a**). Following the same DT and oral OVA administration regimen as above, mice were immunized with OVA+Alum 8 and 15 days after the last DT injection and intranasally challenged with OVA three times in 3-day intervals. Eosinophilia in the bronchoalveolar lavage fluid (BALF) and lung, as well as total lung tissue infiltrate and serum IgE were similarly suppressed in OVA-fed wild-type and MM^{DTR}, but not in zDC^{DTR} mice, when compared to PBS-fed mice of their genotypes (**Fig. 2b-g**). These data show that the absence of cDCs during antigen feeding results into failure to establish tolerance to both T_H1 and T_H2 immunity.

cDCs are required for pT_{reg} cell induction

Oral tolerance is mediated by pT_{reg} cells[2, 3]. We thus addressed whether the pre-DC lineage was required for pT_{reg} cell induction upon antigen feeding by adoptively transferring sorted naïve OVA-specific CD45.1 OT-II cells into APC-depleted BM chimeric mice and assessing the appearance of CD45.1 $Foxp3^+$ T cells in various tissues upon OVA gavage (**Fig. 3a**). DT administration alone did not induce OT-II cell activation, proliferation or differentiation in these chimeric mice (**data not shown**). 48 hours after initial administration of oral OVA MM^{DTR} mice displayed compromised but perceptible pT_{reg} cell induction in mLNs compared to wild-type controls (**Fig. 3b, c**), an effect that was accompanied by an unaltered degree of OT-II cell engraftment, but reduced overall OT-II cell activation and division (**Fig. 3b-f, Supplementary Fig. 2a**). In contrast, pT_{reg} cells were virtually undetectable in OVA-fed zDC^{DTR} mice (**Fig. 3b, c**) and T cell activation was decreased compared to OVA-fed wild-type mice (**Fig. 3e**). OT-II cell engraftment was reduced in zDC^{DTR} mice (**Fig. 3d**), an observation we also made after DT administration alone (**Supplementary Fig. 2b**). At this time-point we did not find significant OT-II cell activation or pT_{reg} cell induction in spleen or distal lymph nodes in any of the groups studied (**data not shown**). The effect of monocyte-macrophage depletion on pT_{reg} cell induction was compensated over time, as by 7.5 days after OVA feeding the frequencies of pT_{reg} cells in MM^{DTR} mice were similar to those in wild-type mice (**Fig. 3g**), in line with the intact tolerance found in these mice. In zDC^{DTR} mice, OT-II cell frequencies 7.5 days after OVA gavage were proportional to the $CD4^+$ T cell compartment (**Supplementary Fig. 2c**), however, pT_{reg} cell frequencies were still severely reduced in mLNs (**Fig. 3g and Supplementary Fig. 2d, e**), spleens and distal lymph nodes (**data not shown**). These data indicate that $CD4^+$ T cell activation, proliferation and pT_{reg} cell induction depend on cDCs and exclude an essential contribution of monocyte-derived APCs to pT_{reg} cell generation upon oral antigen exposure.

$CX3CR1^+$ APC contribution to pT_{reg} cell polarization in mLN

Here we distinguished APC subsets by ontogeny, but others have ascribed roles to gut-associated APCs based upon CX3CR1-targeting approaches[9, 11, 13, 23]. To define the lineage of origin of CX3CR1-expressing APC populations in steady-state mLNs, we generated BM chimeras from *Cx3cr1*$^{+/GFP}$ mice crossed to zDC^{DTR}, MM^{DTR} or wild-type control mice and characterized GFP^+ cell loss upon DT injection. GFP^+ cells represented roughly 25% of all $CD11c^+$ APCs in the mLN (**Fig. 4a, b**). DT administration to MM^{DTR} mice indicated that most monocyte-macrophage–derived cells were among the GFP^+ cells (**Fig. 4b, c**). In addition to $CD64^+$ macrophages, about half of $CD8\alpha^+$ and $CD11b^+$ cells, and roughly 20% of $CD103^+CD11b^-$ populations amongst the GFP^+ cells were depleted by DT in MM^{DTR} mice, indicating that part of the GFP^+CD64^- cells are of monocyte-macrophage origin (**Fig. 4b, c**). Notwithstanding, DT targeting in zDC^{DTR} mice revealed that cDC–derived cells represented the majority of APCs among $CX3CR1^+$ cells (**Fig. 4b, c**). These analyses highlight the heterogeneity of CX3CR1 expression within APC subsets.

Microbiota-derived signals have been implicated in regulation of $CX3CR1^{hi}$ mononuclear phagocyte migration[13]. To better characterize these cells, we transplanted bone marrow from zDC^{DTR} (*Cx3cr1*$^{+/GFP}$) or wild-type *Cx3cr1*$^{+/GFP}$ control mice into germ-free (GF) and specific pathogen free (SPF) wild-type hosts. We found a selective increase of the

CD103^{+}CD11b^{+} population in the mLNs of GF mice compared to SPF mice (**Fig. 4d, Supplementary Fig. 3a**). However, the fraction of CX3CR1^{+} among CD103^{+}CD11b^{+} cells remained the same (**data not shown**), indicating that this enrichment was not explained by specific CX3CR1^{+} cell mobilization. Depletion of cDCs in the zDC^{DTR} (*Cx3cr1*$^{+/GFP}$) chimeras indicated that CD11c^{+}CD64^{-} cells, including migratory subsets, remained pre-DC–derived in GF mice (**Fig. 4d, Supplementary Fig. 3b**). Finally, we asked whether the altered cDC composition in GF mice had an effect on pT$_{reg}$ cell induction. GF hosts displayed reduced pT$_{reg}$ cell induction and cell division in our OT-II transfer system, and DT administration completely prevented Foxp3 upregulation in both GF and SPF zDC^{DTR} hosts (**Fig. 4e**). The reduction in CD4^{+} T cell numbers and OT-II engraftment in zDC^{DTR} mice was comparable under both GF and SPF conditions (**Supplementary Fig. 3c, d)**. These data indicate that the composition of APCs in GF mice is less favorable for pT$_{reg}$ cell induction and that the remaining APCs in cDC-depleted GF hosts cannot rescue the SPF phenotype.

In order to further reconcile our lineage-based approach with CX3CR1-targeting strategies and address the role of CX3CR1^{+} APCs in pT$_{reg}$ cell induction, we performed OT-II adoptive transfer experiments into *Itgax*-Cre × *Cx3cr1*$^{LsL\text{-}DTR}$ (CX3CR1^{DTR}) or *Cx3cr1*$^{LsL\text{-}DTR}$ (wild-type control) BM recipients[13]. In CX3CR1^{DTR} mice, Cre recombinase is under control of the *Itgax* promoter, while DTR is preceded by a *loxP* site-flanked stop cassette under the *Cx3cr1* promoter, allowing DT-mediated depletion of (CD11c^{+}) CX3CR1^{+} cells for at least 48 hours[13]. As previously reported[13], DT administration to CX3CR1^{DTR} mice led to depletion of mLN macrophages (CD11c^{+}CD64^{+}cells), although it also depleted CD11c^{+}CD64^{-} cells (**Fig. 4f**). The degree of depletion in each APC subset (**Fig. 4g**) correlated with the percentage of CX3CR1^{+} cells in these subsets (**Fig. 4a-c**). In line with this pleiotropic APC targeting, pT$_{reg}$ cell induction in CX3CR1^{DTR} mice was more severely reduced than in MM^{DTR} mice (**Fig. 4h** and **Fig. 3c**), while OT-II cell activation and division were only mildly affected and CD4^{+} T cell numbers and OT-II adoption were not altered when compared to wild-type controls (**Fig. 4i** and **Supplementary Fig. 3e, f**). However, similar to what was observed in MM^{DTR} mice, pT$_{reg}$ cell frequencies and OT-II cell division were restored to wild-type levels by day 7.5 post OVA gavage (**Fig. 4i, j**). Taken together, these results suggest that CX3CR1-expressing macrophages are not essential, while cDCs are required for pT$_{reg}$ cell generation by dietary antigen and highlight the merits of a lineage-based approach to dissect differential APC contributions to pT$_{reg}$ cell induction and oral tolerance.

cDCs display differential molecular signatures

Past studies have described pT$_{reg}$ cell-inducing DC populations in the murine gut and gut-draining lymph nodes [6, 7, 8, 10, 16]. Additionally, in recent years, large transcriptome databases for specific cDC populations have been made available[24, 25, 26]. However, these studies did not compare IRF4– versus IRF8–dependent (distinguishable by CD8α^{-}CD11b^{+} or CD8α^{+}CD11b^{-} staining, respectively) among resident and migratory (CCR7^{-} or MHCII^{int} versus CCR7^{+} or MHCII^{hi}) DC populations. To obtain a higher resolution of the cDC subsets and to link them with their lineage of origin, we performed RNA sequencing of cDCs present in the mLNs. We analyzed four CD11c^{+}CD64^{-} subsets: mLN-resident MHCII^{int} (CD8α^{+}CD11b^{low}CD103^{+} and CD8α^{-} CD11b^{+}CD103^{-}) and migratory MHCII^{hi}

(CD11b$^-$CD103$^+$ and CD11b$^+$CD103$^+$) subpopulations. Plasmacytoid DCs (pDCs) were not evaluated due to their very low abundance and the fact that these cells are not targeted in zDC^{DTR} mice. Of note, we observed that the relative frequencies of cDC and lymphocyte subsets were similar in the different lymph nodes draining the proximal to distal gastrointestinal tract (**Supplementary Fig. 4a-m**) and therefore subjected cDCs sorted from total mLN pools to expression profiling. Unsupervised principle component analysis (PCA) revealed that resident and migratory cDC subsets were the most segregated populations (**Supplementary Fig. 4n**), while IRF8– and IRF4–dependent subsets followed a hierarchical pattern in their tolerance-inducing gene expression. As such, migratory, IRF8–dependent CD103$^+$CD11b$^-$ DCs had the highest expression of retinaldehyde dehydrogenase (RALDH2) *Aldh1a2*, as well as *Tgfb2*, *Itgb8* and several other genes associated with generation of pT$_{reg}$ cells and gut-homing. This gene signature was progressively lost by the CD8α$^+$ and CD103$^+$CD11b$^+$ populations, which rather expressed other isoforms of *Tgfb* and *Aldh*; CD11b$^+$ DCs had the lowest expression of these genes (**Fig. 5a-c** and **Supplementary Fig. 4o, p**). This hierarchy was confirmed by the activity of RALDHs in cDCs freshly isolated from total mLNs (**Fig. 5d**). In contrast, CD103$^+$CD11b$^-$ DCs did not express typical pro-inflammatory genes, although *Il12b* (encoding IL-12p40) was preferentially expressed compared to the other DC populations. However, *Il12a* (encoding IL-12p35) or *Il23a* (encoding IL-23p19) were not present in the absence of inflammatory triggers (**Supplementary Fig. 4q**). While CD11b$^+$ DCs showed the lowest pT$_{reg}$ cell-inducing gene signature, they had the highest expression of genes associated with pathogen sensing and initiation of inflammatory responses, including TLRs and TLR-signaling molecules (**Fig. 5a, e**) and a distinct cytokine expression profile (**Supplementary Fig. 4q**). The above expression profiling pointed to IRF8–dependent cDCs as the main tolerogenic subsets in the mLNs.

Zbtb46–driven *Irf8* targeting impacts pT$_{reg}$ cell induction

Several strategies have been devised in the past to ablate BATF3– or IRF8–dependent, or CD11b$^-$ DCs[27, 28, 29, 30], but some approaches led to defects beyond those caused by loss of cDC subsets[28, 31]. Recently, additional cDC-specific genetic approaches have been reported[32, 33] and they revealed the reliance of T helper polarization on certain DC populations [20]. However, whether a specific cDC subset is necessary for pT$_{reg}$ cell induction and oral tolerance has not been addressed. We therefore generated a mouse strain expressing Cre under the endogenous *Zbtb46* promoter (zDC^{Cre})[34] and crossed it to mice with a *loxP* site flanked exon 2 of the *Irf8* gene, encoding the DNA binding domain of this transcription factor (zDC(Δ*Irf8*) mice)[35]. The mice were viable, born at Mendelian ratios, and exhibited normal weights and no visible pathologies up to the age of twelve weeks. This strategy led to the loss of CD8α$^+$ and CD11b$^-$ cDCs in mLN, lamina propria (**Fig. 6a-e**) and spleen (**Supplementary Fig. 5a-c**) of zDC(Δ*Irf8*) compared to *Irf8*$^{fl/fl}$ mice, with no major effects on T or B cell frequencies (**Fig. 6f, g** and **data not shown**). We noticed that excision of *Irf8*[35] led to variable loss of cDCs; however, since this property appeared conserved among BM recipients, BM transplant preserved the degree of niche depletion and permitted the generation of large and uniform cohorts of CD8α$^+$ and CD11b$^-$ cDC-deficient mice.

We therefore utilized zDC(Δ*Irf8*) BM chimeras to assess the importance of IRF8–dependent cDCs for oral tolerance (**Fig. 1b**, excluding DT injection). We found that ear swelling, IgG1 and IgG2c amounts in the serum were suppressed to a similar degree in zDC(Δ*Irf8*) and *Irf8*$^{fl/f}$ control BM recipient mice compared to the PBS-fed mice of each genotype (**Fig. 7a-c**). This apparently intact tolerance in zDC(Δ*Irf8*) mice was observed even when we immunized with OVA+CFA 24 hours after the first oral antigen encounter to blunt potential compensatory pT$_{reg}$ cell expansion (**data not shown**). Next, we directly assessed the importance of IRF8–dependent cDCs for pT$_{reg}$ cell polarization upon oral antigen *in vivo*. 48 hours after first oral OVA encounter, pT$_{reg}$ cell induction of adoptively transferred naïve OT-II cells was lower in zDC(Δ*Irf8*) than in *Irf8*$^{fl/f}$ mice, while cell division was significantly increased (**Fig. 7d-f**). This phenomenon persisted in mLN, spleen and other peripheral lymph nodes at 7.5 days after OVA feeding (**Fig. 7g** and **data not shown**). OT-II cells did not produce significant amounts of IFN-γ, IL-5 or IL-17a under these conditions, and this was not increased in zDC(Δ*Irf8*) mice (**data not shown**). These findings were in line with the loss of the migratory and resident mLN DC subsets with the most tolerogenic signatures. However, the impairment in pT$_{reg}$ cell induction was less severe than in zDC^{DTR} mice, indicating that the remaining cDC pools could compensate for the IRF8–DC lineage loss during oral tolerance development. These results demonstrate that the targeting of IRF8–dependent cDCs partially prevents pT$_{reg}$ cell generation *in vivo* but does not affect oral tolerance, indicating that the remaining cDC pools and pT$_{reg}$ cells could compensate for the IRF8–DC lineage loss.

Hierarchical roles of cDCs in pT$_{reg}$ cell induction

To gain insights into early changes imprinted on T cells by different DC populations, we performed RNA sequencing analyses of activated OT-II cells upon 24 hours of co-culture with mLN-derived cDC subsets and OT-II peptide. Unsupervised PCA indicated that OT-II cells stimulated by resident and migratory cDC subsets were the most segregated populations (**Supplementary Fig. 6**), analogous to the clustering of DC subsets (**Supplementary Fig. 4n**). The various cDC subsets induced a hierarchical pT$_{reg}$ cell pattern in OT-II cells (**Fig. 8a**). Consistent with the cDC gene profile (**Fig. 5a-c**), and with a process initiated by the TGF-β and RA pathways[6, 7, 8, 16, 17, 36], naïve T cells upregulated several pT$_{reg}$ cell– and gut homing–associated genes when exposed to CD103^{+}CD11b^{-} DCs; CD103^{+}CD11b^{+} and CD8α^{+} induced an intermediary phenotype and CD11b^{+} DCs were the poorest in triggering this signature (**Fig. 8a, b**). The pT$_{reg}$ cell-polarizing capacity of mLN cDCs subsets was confirmed in co-culture experiments without addition of exogenous TGF-β and RA[6]: CD11b^{-}CD103^{+} cells were the most efficient inducers, followed by CD8α^{+}, CD11b^{+}CD103^{+} and CD11b^{+}CD103^{-} cells (**Fig. 8c**), results that closely mirrored the cDC subset and OT-II transcriptome analyses. Although the frequencies of activated OT-II cells were similar upon co-cultures with the different DC subset (**data not shown**), we found an inverse correlation between pT$_{reg}$ cell- versus proliferation-induction among cDC subsets, whereby CD8α^{-}CD11b^{+} cells triggered the highest rate of cell division (**Fig. 8c**). Since the provision of antigen *in vitro* may obscure differences in antigen capture and processing that occur *in vivo*, we also examined pT$_{reg}$ cell polarization in co-cultures with cDCs sorted from OVA-fed mice. We found that CD11b^{-}CD103^{+} cells consistently induced a higher frequency of Foxp3^{+} OT-II cells, although other cDC subsets were also able to induce Foxp3 (**Fig. 8d**).

Overall, the differences in pT_{reg} cell induction potential among the cDC subsets correlated with lineage but not strictly MHC class II expression: $CD11b^{-}$ DC subsets provided superior pT_{reg} cell polarizing and inferior cell cycling or pro-inflammatory signals over the $CD11b^{+}$ subsets, corresponding to the IRF8– and IRF4–dependent cDC lineages, respectively. In conclusion, we observed that cDC subsets play a hierarchical, but redundant role in pT_{reg} cell induction and oral tolerance.

Discussion

Here we report that pre-DC– but not monocyte–derived APCs are required for both, generation of pT_{reg} cells and oral tolerance. In addition, pre-DC–derived cDC subsets play partially-redundant roles in these processes, with IRF8–dependent cDC populations being the primary pT_{reg} cell inducers. Our high-resolution analysis of cDCs subsets identified a pT_{reg} cell-inducing gene signature in the IRF8-dependent, $MHCII^{hi}CCR7^{hi}$ migratory cDC population, which is consistent with the established role of $CD103^{+}$ DCs[6, 10] for pT_{reg} cell polarization. By using ontogeny-based genetics, we provide evidence to reconcile previous observations defining APC requirements for pT_{reg} cell induction using various cell surface-based targeting strategies. Because major APC subsets were depleted specifically only during oral antigen exposure, our studies do not rule out a role for monocyte-derived lineages or pDCs in the maintenance, expansion and survival of pT_{reg} cells during later phases of oral tolerance formerly suggested[9, 37].

Cell-surface molecules such as CCR2, CD11c and CX3CR1 have been used as targets to ablate APC function, development or migration in multiple studies aimed at defining a role for these cells in pT_{reg} cell induction[9, 11, 13, 15, 38, 39]. Given the high expression of CX3CR1 by intestinal APCs, two main strategies targeted CX3CR1-expressing cells or *Cx3cr1* itself[13, 23]. Receptor targeting studies using *Cx3cr1*$^{GFP/GFP}$ mice inferred that CX3CR1 is necessary for luminal antigen sampling and transfer[11, 23], suggesting an essential role of fractalkine sensing for APC function and/or localization. A study using cell-transfer strategies concluded that CX3CR1 was required for macrophage-mediated pT_{reg} cell expansion rather than pT_{reg} cell induction[9], and these results are not in contradiction to our observations. More recently, $CX3CR1^{hi}$ APCs were defined as lamina propria and mLN macrophages, while a fraction of DCs from pre-DC origin was reported to express low or intermediate levels of CX3CR1[13, 32, 40, 41, 42]. A study targeting APCs by DT administration to $CX3CR1^{DTR}$ mice showed that while $CX3CR1^{hi}$ mononuclear phagocytes were efficiently deleted, $CX3CR1^{lo/int}$ cells (non-macrophages) remained intact in the lamina propria[13]. Both by $CX3CR1^{GFP/+}$ reporter analysis and lineage depletion strategies, we determined the contribution of macrophages and cDC subsets to the $CX3CR1^{+}$ pools in mLN and lamina propria. We observed depletion of both macrophages and CX3CR1-expressing cDCs in the mLNs of $CX3CR1^{DTR}$ BM recipient mice upon DT administration. Regardless of apparent targeting differences, we did not find sustained impairment of pT_{reg} cell induction in DT-injected $CX3CR1^{DTR}$, in line with our observation that monocyte-derived APCs are not strictly needed for oral antigen-mediated pT_{reg} cell induction. However, it remains to be resolved whether CX3CR1-expressing cells play a specific role in the maintenance of pT_{reg} cells and oral tolerance, or, alternatively, whether CX3CR1 receptor expression is required for functional and anatomical properties of cDCs.

Lineage-based intersectional genetics also provided important information regarding a hierarchy of cDC subsets in their pT_{reg} cell induction potential. IRF8–dependent cDCs, the $CD8\alpha^+$ or the $CD103^+CD11b^-$ cDCs populations[43, 44], were highly efficient in pT_{reg} cell generation. Our transcriptomics results confirmed and expanded previous analyses[24, 25], identifying that TGF-β and RA pathways are highly enriched in migratory $CD103^+CD11b^-$ DCs. Furthermore, while our data corroborate earlier observations that $CD103^+$ DCs are efficient pT_{reg} cell inducers via these pathways, they also identify the subpopulation amongst the three $CD103^+$ DC populations in the mLN ($CD8\alpha^+CD11b^{low}CD103^+$, $CD11b^-CD103^+$ and $CD11b^+CD103^+$) governing this phenomenon. Parallel T cell and cDC RNA-seq also revealed cDC subset-specific gene signatures that closely mirror early gene programs induced in T cells, further reinforcing the role of these pathways in the generation of pT_{reg} cells[2, 4, 6, 7, 8].

In line with previous studies addressing the role of IRF4 and Notch2 in the development of cDCs[26, 45, 46, 47, 48], we observed that $CD11b^+$ DCs subsets were rather inefficient in pT_{reg} cell induction, while they showed a superior capacity in the expansion and maintenance of $CD4^+$ T cells and polarization towards helper T cells. The preference of particular cDC subsets in inducing pT_{reg} cell versus effector T cell differentiation was not absolute, as demonstrated by our *Irf8*– targeting approach that resulted in reduced pT_{reg} cell generation but intact oral tolerance. Our observations support recent reports that indicate a division of labor among APC subsets [13, 49]. However, depletion of the microbiome, which has been shown to boost the migratory capacity of intestinal APCs[13], did not rescue pT_{reg} cell induction in mice depleted of cDCs. Additionally, although migratory IRF8–dependent cDCs appeared to have the highest capacity to induce pT_{reg} cell differentiation in the mLN, this subset is underrepresented in the lamina propria. This observation, along with known cell-free antigen distribution through the intestinal draining lymph[50], raises the possibility that antigen sampling and carriage may have only a limited impact when compared to cell-independent pathways of antigen distribution; rather, what determines the degree of pT_{reg} cell induction is the composition of cDCs in the mLN that capture antigen *in situ*. Therefore, the characterization of the relative contribution APC-mediated *versus* cell-free antigen delivery is a logical next step for these studies.

Online Methods

Mice

C57BL/6J CD45.1 (B6.SJL-Ptprca Pepcb/BoyJ) and CD45.2 (C57BL/6J), *Lyz2*$^{Cre/Cre}$ (B6.129P2-Lyz2tm1(cre)Ifo/J), *Cx3cr1*^{GFP} (B6.129P(Cg)-Ptprca Cx3cr1tm1Litt/LittJ), *Cx3cr1*$^{LsL\text{-}DTR}$ (B6N.129P2-Cx3cr1tm3(DTR)Litt/J), $CD11c^{Cre}$ (B6.Cg-Tg(Itgax-cre)1-1Reiz/J), $CD11c^{DTR}$ (B6.FVB-Tg(Itgax-DTR/EGFP)57Lan/J) and *Irf8*$^{fl/fl}$ (B6(Cg)-*Irf8*tm1.1Hm/J) mice were purchased from the Jackson Laboratories and CD45.1 OT-II TCR-transgenic were originally purchased from Taconic Farms and maintained in our facilities. *Csf1r*$^{LsL\text{-}DTR}$, zDC^{DTR} and zDC^{Cre} knockin mice were generated in the Nussenzweig lab and generously shared with us[20, 21, 34]. These lines were interbred in our facilities to obtain the final strains described in the text. Genotyping was performed according to the protocols established for the respective strains by Jackson Laboratories.

zDC^{Cre} mice were screened for Cre using PCR primers: 5'-TTACCGGTCGATGCAACGAGT-3' and 5'- TTCCATGAGTGAACGAACC-3'. Excision of the floxed *Irf8* allele fragment was confirmed using Platinum DNA polymerase (Invitrogen) and primers 5'-TTGGGGATTTCCAGGCTGTTCTA-3' and 5'-TCTACACAGGAAGCAAGCCG-3', which give rise to ~2900 bp or ~1500 bp PCR product for the floxed or recombined *locus*, respectively. Mice were used at 7-12 weeks of age, and male mice were used throughout the study unless indicted otherwise. Mice were maintained at the Rockefeller University animal facilities under specific pathogen-free conditions or germ free conditions. Germ-free C57BL/6 mice were generously provided by S. Mazmanian (Caltech) and imported into germ-free flexible film isolators (Class Biologically Clean Ltd.). The mice were bred in our germ-free facility for maintenance of the strain and kept on sterilized Autoclavable Mouse Breeder Diet (5021, LabDiet, USA), which was also used for control (ex germ-free) SPF mice. Animal care and experimentation were consistent with the NIH guidelines and were approved by the Institutional Animal Care and Use Committee at the Rockefeller University.

Antibodies and cell staining

Antibodies are described in the **Supplementary table 1**. Aqua LIVE/DEAD® Fixable Aqua Dead Cell Stain Kit, L-34965, was purchased from Life Technologies. Horseradish peroxidase conjugated Streptavidin was purchased from Jackson ImmunoResearch Laboratories, Inc.

Lymphocyte and APC isolation from small intestine

Small intestines were separated from mesentery, and Peyer's Patches and feces were removed. Intestines were cut longitudinally and washed twice in Magnesium and Calcium free HBSS+ 1 g/l glucose (HBSS) (Gibco), and once in HBSS + 1 mM DTT (Sigma-Aldrich). Tissue was cut into 1 cm pieces and the epithelium removed by incubation in 25 ml of HBSS + 2% FCS + 1.3 mM EDTA for 15 min at 37°C at 230 rpm. Tubes were vortexed, the intestinal pieces recovered in a sieve and washed for an additional 15 min in 25 ml of HBSS + 2% FCS at 37°C at 230 rpm. Tissues were then finely chopped and digested in 8 ml of RPMI (Gibco), 2% FCS, 200 μg/ml DNaseI (Roche) and 2 mg/ml Collagenase IV (Gibco) for 2× 20 min at 37°C, 5% CO_2. After the first and second 20 min, digests were taken up and resuspended 10 times. Final digests were passed through a sieve and the collagenase quenched by addition of 15 ml of cold RPMI, 2% FCS. Cell pellets were resuspended in 35% Percoll (BD Pharmigen), passed through a 100 μm mesh and separated by centrifugation in a discontinuous Percoll gradient (70%/35%) at 1000 *g* for 25 min at room temperature (RT). APCs and lymphocytes were isolated from the interphase, washed, and stained for FACS analysis.

Lymphocyte and APC isolation from lymph nodes and spleen

Tissues were dissected into cold HBSS supplemented with Mg^{2+} and Ca^{2+}, finely chopped and incubated in 400 U/ml Collagenase D (Roche) in HBSS for 25 min at 37°C, 5% CO_2. Collagenase was quenched on ice by addition of final 10% FCS. Single cell suspensions

were extracted from connective tissue by taking up and resuspending the digests five times. Erythrocytes were lysed by incubation in erythrocyte lysis buffer (Sigma) for 7 min at RT.

Segmentation of mesenteric lymph nodes

Mesenteric lymph nodes draining intestinal segments were determined anatomically by following the lymphatic vessels connecting the colon, ileum and jejunum to their lymph nodes. Duodenal lymph nodes were revealed by gavaging 100 μl of olive oil (Sigma) and determining the most stomach-proximal lymph nodes surrounded by chyle, indicative of duodenal drainage, 2 h post gavage. Non-chylous stomach-proximal lymph nodes (celiac and pancreatic) were excluded from total mLN analyses.

Cell sorting

Cells were sorted using FACS Aria cell sorter flow cytometer (Becton Dickinson). For mesenteric dendritic cell sorting, cells were pre-enriched using anti-CD11c MACS beads (Miltenyi Biotec) and LS MACS Separation Columns (Miltenyi Biotec). Dendritic were sorted as $Aqua^{-}CD45^{+}Lin^{-}(CD3^{-}B220^{-}NK1.1^{-}CD19^{-})$ $CD11c^{hi}$, and the subpopulations further as $MHCII^{int}CD8\alpha^{+}CD11b^{lo}$, $MHCII^{int}CD8\alpha^{-}CD11b^{+}$, $MHCII^{hi}CD103^{+}CD11b^{-}$ and $MHCII^{hi}CD103^{+}CD11b^{+}$. Naïve CD4 T cells were pre-enriched by negative selection using biotinylated antibodies against CD8α, CD25, CD11c, CD11b, TER-119, NK1.1, and B220 and anti-biotin MACS beads (Miltenyi Biotec) and sorted as $Aqua^{-}CD11c^{-}CD8\alpha^{-}MHCII^{-}V\alpha2^{+}CD4^{+}CD25^{-}CD62^{hi}CD44^{lo}$.

FACS analysis

Cell populations were stained with Aqua in PBS, followed by incubation with Fc block and antibodies against the indicated cell surface markers in FACS buffer (PBS, 1% BSA, 10 mM EDTA, 0.02% sodium azide). The cells were analyzed live, or fixed in 1% PFA/PBS. For Foxp3 staining analysis, surface staining was followed by permeabilization using Foxp3 Mouse Regulatory T cell Staining Kit (eBioscience). FACS data was acquired on a LSR-II flow cytometer (Becton Dickinson) and analyzed using FlowJo software package (Tri-Star). Cell division index was calculated using the FlowJo formula (http://www.flowjo.com/v765/en/proliferation.html), whereby the index represents the fraction of total cell divisions over the calculated total starting cells. Note that calculation of the division index is based on cells present at the time of analysis and cannot take into account potential lack of survival of CD45.1 cells in zDC^{DTR} BMCs. Lineage contributions to APC pools (Fig. 4 a, b) were calculated on the assumption that DT-mediated depletion was 100% efficient: First, we determined the frequency of each APC subpopulation in DT-treated wild-type mice; next, we determined the frequency of each subpopulation in DT-treated zDC^{DTR} (and MM^{DTR}) mice; finally, because depletion is not 100% and every mouse has slightly different APC subpopulation ratios (routinely +/− 5% for all cDC populations), we calculated the relative contribution for cDC- (or MM-) targeted to the wild-type levels to draw pie charts.

Bone marrow chimeras

Bone marrow recipients were irradiated with two doses of 525 rad 3 h apart, and received $2\text{-}5\times10^{6}$ bone marrow cells by retro-orbital injection under isoflurane anesthesia. Bone

marrow chimeras were reconstituted for a minimum of eight weeks after irradiation before the start of their experimental use. Germ-free bone marrow recipients were exported and irradiated in a sterile container, injected under a sterile hood and re-imported into sterile isolators. Mice tested negative for contamination 4 weeks after re-import and at the end of the experiments. For studies comparing *Irf8*$^{fl/fl}$ and *zDC*(Δ*Irf8*) bone marrow recipients, the *Irf8*$^{fl/fl}$ bone marrow was obtained from the pure *Irf8*$^{fl/fl}$ strain.

Diphtheria toxin (DT) administration

The first dose of DT (Sigma, D0564) was delivered intraperitoneally (i.p.) as 500 ng in 200 μl PBS/ 20 g body weight followed by one or two doses of 100 ng in 200 μl PBS/ 20 g body weight, as indicated. Depletion efficiency was monitored in each animal by the serum Flt3L surge upon cDC depletion (zDC^{DTR}) and the loss of blood monocytes 24h post DT administration in MM^{DTR} mice.

Anti-Flt3L ELISA—Serum concentrations of Flt3L were determined using an anti-Flt3L ELISA kit (R& D Systems) according to the manufacturer's protocol. Sera were diluted 1:4 to be in range of the standard curve.

Oral antigen administration

OVA (grade III, Sigma, A5378) was administered at 50 mg in 200 μl PBS by oral gavage using metal gavage needles.

^{125}Iodine labeling of ovalbumin and ^{125}I-OVA uptake and clearance analysis

OVA grade VII (Sigma, A7641) was labeled with ^{125}Iodine (Perkin-Elmer) under a fume hood. Briefly, 250 μCi Na^{125}I in 135.5 μl 0.1 N NaOH was prepared and immediately mixed with an equal volume of 0.1 N HCl containing 6.67 nmol ICl. The iodine mixture was immediately added to 1 ml of 100 μg OVA in 1M glycine, pH 9.5, 100 mM NaCl (2.26 μM OVA, equivalent to an Iodine: OVA molar ratio of 3:1), and the solution incubated at RT for 10 min. Unincorporated iodine was removed by purifying the sample on two consecutive NAP25 columns (GE Healthcare). ^{125}I-OVA was eluted in H_2O and kept at 4 °C in 1× PBS by appropriate addition of 10× PBS. Amount of labeling was determined on a Packard Cobra gamma counter and an estimated to be 95000 CPM/μg OVA. Protein purity and integrity were confirmed on a Coomassie gel and specific labeling of OVA by exposing the gel to autoradiography film. To determine OVA uptake and clearance, mice were fasted for 3 h and then gavaged at 12 pm with 50 mg OVA grade III in 200 μl PBS 300,000 CPM ^{25}I-OVA (about 3 μg OVA). Submandibular blood and urine were collected in 5 μl aliquots; whole organs were taken at indicated time points and weighed. Radioactivity was measured using on a Packard Cobra gamma counter.

CFA immunization and subcutaneous ear challenge

Eight days after oral OVA gavage, CFA-OVA was administered subcutaneously between the shoulder blades as an emulsion of 100 μl CFA and 100 μl PBS containing 300 μg endotoxin free OVA (EndoGrade® Endotoxin-free Ovalbumin, HYGLOS, Germany, 321000) under isofluorane gas anesthesia. The first ear challenge was performed 14 days after

immunization. 2.5 mg/ml endotoxin free OVA was heat aggregated in PBS at for 2 h at 65 °C, and 30 μl of OVA (left ear) or PBS vehicle (right ear) were injected under isofluorane gas anesthesia. Ear thickness was measured using a digital precision caliper (Fisher Scientific). Swelling was determined by first subtracting pre-challenge from post-challenge ear thickness, and then subtracting the swelling upon PBS injection from swelling upon OVA injection.

Alum immunization and airway challenge

Eight days after oral OVA administration, 4 ug of endotoxin-free OVA antigen adsorbed to 40 μl Imject™ Alum Adjuvant (Fisher Scientific) was injected i.p. in a final volume of 400 μl made up with PBS. Immunization was repeated after 7 days. To induce airway inflammation, mice were anesthetized and intranasally administered 10 ug of endotoxin-free OVA in 50 μl PBS (25 μl per nostril) on days 14, 17 and 21 after the first i.p. immunization.

Bronchoalveolar Lavage (BAL), lung histology and infiltrate analysis by flow cytometry

Mice were anesthetized by i.p. injection of 0.35 ml of 2.5% avertin (Sigma), the trachea was cannulated and lungs were lavaged with once with 0.5 ml and then 1.0 ml PBS. Total BAL cells were counted after erythrocyte lysis and stained for FACS analysis. Lungs were perfused via the right ventricle with 10 ml saline to wash out residual blood. One lobe was digested in 400 U/ml collagenase D/HBSS and processed for FACS analysis. Eosinophils were determined as $CD45^{+}SSA^{hi}MHCII^{-}CD11b^{+}Ly6G^{int}SiglecF^{+}$. Another lobe was fixed with 4% phosphate-buffered formalin and embedded in paraffin. Tissues sections were stained with hematoxylin/eosin (H&E) to determine cellular inflammation. Sections where assessed in a blinded fashion. An infiltration score was created whereby 0=no, 1=very mild, 2=mild, 3=locally severe, 4=uniformly severe, 5=uniformly very severe infiltration was observed in a 1 cm^2 section.

Anti-OVA IgG1 and IgG2c ELISAs

High binding ELISA 96-well plates (Corning, 3690) were coated with 50 μl of 20 μg/ml OVA grade II in 100 mM Na_2CO_3 overnight at 4°C. Plates were washed three times PBS-0.05% Tween 20 (PBS-T, Sigma), and blocked with 150 μl 1% BSA in PBS-T for 2 h at RT. Mouse sera were obtained by submandibular bleeding and diluted in blocking buffer and added as 25 μl/ well. For anti-OVA IgG1 ELISA quantification, an anti-OVA IgG1 (Biolegend) standard curve ranging from 0.125 to 8 ng/ml was applied; for anti-OVA IgG2c ELISA quantification, a hyper-immune serum was diluted ranging from a 1:7500 (set as 1.0) to 1:480,000 (set as 0.0156) dilution and the 1:7500 concentration set as 1. Sera were measured in duplicates and at two dilutions, typically 1:500,000 and 1:2,000,000 for the anti-IgG1 ELISA, and 1:5000 and 1:20,000 for the anti-IgG2c ELISA. Standards and test sera were incubated for 1 h at RT and the plates washed three times in wash buffer. Biotinylated anti-IgG1 or anti-IgG2c applied as 50 μl at 20 ng/ml in blocking buffer, the plates incubated for 1 h and washed four times. Horseradish peroxidase linked Streptavidin (HRP-Streptavidin) was added as 50 μl at 40 ng/ml and the plates incubates for 45 min at RT and then washed five times. Fifty μl HRP substrate TMB was added and the reaction stopped by addition of 50 μl 1N H_2SO_4. Plates were read at $A_{450\text{-}570nm}$. Absolute concentrations of anti-OVA IgG1 were determined from the standard curve; relative concentrations of anti-

OVA IgG2c were determined by dividing the concentrations determined by the standard curve by 4,800.

Anti-IgE ELISA

High binding ELISA 96-well plates (Corning, 3690) were coated with 50 μl of 2μg/ml anti-IgE antibody (Invitrogen) in 100 mM Na_2CO_3 overnight at 4°C. Plates were washed three times PBS-0.05% Tween 20 (PBS-T, Sigma), and blocked with 1 μl 1% BSA in PBS-T for 2 h at RT. Mouse sera were diluted in blocking buffer (typically 1:2 and 1:20) and added as 25 μl/ well in duplicates. An IgE isotype control standard curve was applied at concentrations from 4 to 256 ng/ml. Standards and test sera were incubated for 2 h at RT and the plates washed three times in wash buffer. Biotinylated anti-IgE was applied as 50 μl at 33 ng/ml, the plates were incubated for 1 h and washed four times. Horseradish peroxidase linked Streptavidin (HRP-Streptavidin) was added as 50 μl at 100 ng/ml and the plates incubates for 45 min at RT and then washed five times. Fifty μl HRP substrate TMB was added and the reaction stopped by addition of 50 μl 1N H_2SO_4. Plates were read at $A_{450\text{-}570nm}$. Absolute concentrations of serum IgE levels were determined from the standard curve.

Adoptive T cell transfer

Sorted naïve CD45.1 OT-II T cells were labeled using the Cell Trace™ Violet Cell Proliferation Kit (C-34557, Life Technologies). 2×10^6 or 6×10^6 cell were transferred by retro-orbital injection under isofluorane gas anesthesia for analyses of cells 48 h or 7.5 days after OVA gavage, respectively,.

***In vitro* T-cell and DC co-culture—**Sorted and Cell Trace™ stained naïve OT-II cells were cultured for 3 days in flat bottom 96 well plates OT-II in the presence of sorted mLN DC subpopulations, 1 μg/ml anti-IL4 and 1 μg/ml anti-IFN-γ antibody. Antigen was either provided as 1 μg/ml of OT-II peptide (chicken OVA323-339, amino acid sequence ISQAVHAAHAEINEAGR, made by the Rockefeller University Proteomics Resource Center), or by *in vivo* loading of DCs by maintaining donor mice on a 20% OVA diet for 2 days and gavaging them with 50 mg OVA 4h prior to mLN isolation. Cells were co-cultured at a 5:1 T cell/DC ratio (100,000 to 20,000 or 50,000 to 10,000).

RALDH activity assay—RALDH activity was determined using the Aldefluor kit (STEMCELL™ Technologies) according to the manufacturer's protocol, with a few optimizing modifications: 3×10^6 cells were incubated at 1×10^6 cells/ml, and were pre-incubated with 30 μM DEAB (Sigma) or vehicle for 30 min at 37°C prior to the addition of 5 μl /ml Aldefluor reagent for a further 30 min.

RNA preparation and RNA sequencing

RNA from sorted cell pellets was extracted and column-purified using the Arcturus PicoPure RNA Isolation kit (Applied Biosystems). Genomic DNA was removed by on-column digest with DNAse I (Qiagen), according to the PicoPure RNA Isolation kit manual. RNA libraries were prepared using the SMARTer Ultra Low Input RNA for Illumina Sequencing kit (Clontech Laboratories) and sequenced using 50 base pair paired end reading on a HiSeq 2500 instrument (Illumina). The reads were aligned using the STAR version 2.3.0 software

that permits unique alignments to Mouse Ensembl genes. Differential expression was determined by use of the Cufflinks software with default settings. Heat maps were generated by comparing the expression profile $CD11b^+$ and $CD103^+CD11b^-$ DCs, or of OT-II cells cultured with $CD11b^+$ and $CD103^+CD11b^-$ DCs. Gene clusters were determined using Gene Set Enrichment Analysis (GSEA v2.2.2) software. PCA was performed using R software.

Statistics—Statistical analysis was performed in GraphPad Prism software. Data was analyzed by applying one-way ANOVA or two-tailed unpaired Student's t-test whenever necessary. For analysis of histological scores non-parametric Mann Whitney test was used. A P value of less than 0.05 was considered significant.

Supplementary Material

Refer to Web version on PubMed Central for supplementary material.

Acknowledgements

We are indebted to M. Amoury and L. Cohn for having put thought into the project in its beginnings; to M. Nussenzweig for generously sharing resources and conceptual input; to B. Reis and V. Pedicord for assistance in mouse dissection experiments, critical discussion and help in preparing the manuscript; K. Velinzon and N. Thomas for assistance in cell sorting; The Rockefeller University Genomics Center; A. Rogoz, T. Rendon, S. Gonzalez and the Rockefeller University Comparative Bioscience Center for good animal care and genotyping; and the New York University histology core for lung histological staining. Supported by a Swiss National Foundation Advanced Postdoc fellowship (D.E.), a National Institutes of Health 1R56AI119062 grant (D.M.), and by the Leona M. and Harry B. Helmsley Charitable Trust (D.E. and D.M.).

References

1. Kretschmer K, Apostolou I, Hawiger D, Khazaie K, Nussenzweig MC, von Boehmer H. Inducing and expanding regulatory T cell populations by foreign antigen. Nat Immunol. 2005; 6(12):1219–1227. [PubMed: 16244650]
2. Mucida D, Kutchukhidze N, Erazo A, Russo M, Lafaille JJ, Curotto de Lafaille MA. Oral tolerance in the absence of naturally occurring Tregs. J Clin Invest. 2005; 115(7):1923–1933. [PubMed: 15937545]
3. Curotto de Lafaille MA, Kutchukhidze N, Shen S, Ding Y, Yee H, Lafaille JJ. Adaptive Foxp3+ regulatory T cell-dependent and -independent control of allergic inflammation. Immunity. 2008; 29(1):114–126. [PubMed: 18617425]
4. Josefowicz SZ, Niec RE, Kim HY, Treuting P, Chinen T, Zheng Y, et al. Extrathymically generated regulatory T cells control mucosal TH2 inflammation. Nature. 2012; 482(7385):395–399. [PubMed: 22318520]
5. Ostroukhova M, Seguin-Devaux C, Oriss TB, Dixon-McCarthy B, Yang L, Ameredes BT, et al. Tolerance induced by inhaled antigen involves CD4(+) T cells expressing membrane-bound TGF-beta and FOXP3. J Clin Invest. 2004; 114(1):28–38. [PubMed: 15232609]
6. Coombes JL, Siddiqui KR, Arancibia-Carcamo CV, Hall J, Sun CM, Belkaid Y, et al. A functionally specialized population of mucosal CD103+ DCs induces Foxp3+ regulatory T cells via a TGF-beta and retinoic acid-dependent mechanism. J Exp Med. 2007; 204(8):1757–1764. [PubMed: 17620361]
7. Mucida D, Park Y, Kim G, Turovskaya O, Scott I, Kronenberg M, et al. Reciprocal TH17 and regulatory T cell differentiation mediated by retinoic acid. Science. 2007; 317(5835):256–260. [PubMed: 17569825]
8. Sun CM, Hall JA, Blank RB, Bouladoux N, Oukka M, Mora JR, et al. Small intestine lamina propria dendritic cells promote de novo generation of Foxp3 T reg cells via retinoic acid. J Exp Med. 2007; 204(8):1775–1785. [PubMed: 17620362]

9. Hadis U, Wahl B, Schulz O, Hardtke-Wolenski M, Schippers A, Wagner N, et al. Intestinal tolerance requires gut homing and expansion of FoxP3+ regulatory T cells in the lamina propria. Immunity. 2011; 34(2):237–246. [PubMed: 21333554]
10. Annacker O, Coombes JL, Malmstrom V, Uhlig HH, Bourne T, Johansson-Lindbom B, et al. Essential role for CD103 in the T cell-mediated regulation of experimental colitis. J Exp Med. 2005; 202(8):1051–1061. [PubMed: 16216886]
11. Mazzini E, Massimiliano L, Penna G, Rescigno M. Oral tolerance can be established via gap junction transfer of fed antigens from CX3CR1(+) macrophages to CD103(+) dendritic cells. Immunity. 2014; 40(2):248–261. [PubMed: 24462723]
12. Farache J, Koren I, Milo I, Gurevich I, Kim KW, Zigmond E, et al. Luminal bacteria recruit CD103+ dendritic cells into the intestinal epithelium to sample bacterial antigens for presentation. Immunity. 2013; 38(3):581–595. [PubMed: 23395676]
13. Diehl GE, Longman RS, Zhang JX, Breart B, Galan C, Cuesta A, et al. Microbiota restricts trafficking of bacteria to mesenteric lymph nodes by CX(3)CR1(hi) cells. Nature. 2013; 494(7435):116–120. [PubMed: 23334413]
14. Worbs T, Bode U, Yan S, Hoffmann MW, Hintzen G, Bernhardt G, et al. Oral tolerance originates in the intestinal immune system and relies on antigen carriage by dendritic cells. J Exp Med. 2006; 203(3):519–527. [PubMed: 16533884]
15. Schulz O, Jaensson E, Persson EK, Liu X, Worbs T, Agace WW, et al. Intestinal CD103+, but not CX3CR1+, antigen sampling cells migrate in lymph and serve classical dendritic cell functions. J Exp Med. 2009; 206(13):3101–3114. [PubMed: 20008524]
16. Iwata M, Hirakiyama A, Eshima Y, Kagechika H, Kato C, Song SY. Retinoic acid imprints gut-homing specificity on T cells. Immunity. 2004; 21(4):527–538. [PubMed: 15485630]
17. Johansson-Lindbom B, Svensson M, Pabst O, Palmqvist C, Marquez G, Forster R, et al. Functional specialization of gut CD103+ dendritic cells in the regulation of tissue-selective T cell homing. J Exp Med. 2005; 202(8):1063–1073. [PubMed: 16216890]
18. Idoyaga J, Fiorese C, Zbytnuik L, Lubkin A, Miller J, Malissen B, et al. Specialized role of migratory dendritic cells in peripheral tolerance induction. J Clin Invest. 2013; 123(2):844–854. [PubMed: 23298832]
19. Yamazaki S, Dudziak D, Heidkamp GF, Fiorese C, Bonito AJ, Inaba K, et al. CD8+ CD205+ splenic dendritic cells are specialized to induce Foxp3+ regulatory T cells. J Immunol. 2008; 181(10):6923–6933. [PubMed: 18981112]
20. Schreiber HA, Loschko J, Karssemeijer RA, Escolano A, Meredith MM, Mucida D, et al. Intestinal monocytes and macrophages are required for T cell polarization in response to Citrobacter rodentium. J Exp Med. 2013; 210(10):2025–2039. [PubMed: 24043764]
21. Meredith MM, Liu K, Darrasse-Jeze G, Kamphorst AO, Schreiber HA, Guermonprez P, et al. Expression of the zinc finger transcription factor zDC (Zbtb46, Btbd4) defines the classical dendritic cell lineage. J Exp Med. 2012; 209(6):1153–1165. [PubMed: 22615130]
22. Jung S, Unutmaz D, Wong P, Sano G, De los Santos K, Sparwasser T, et al. In vivo depletion of CD11c+ dendritic cells abrogates priming of CD8+ T cells by exogenous cell-associated antigens. Immunity. 2002; 17(2):211–220. [PubMed: 12196292]
23. Niess JH, Brand S, Gu X, Landsman L, Jung S, McCormick BA, et al. CX3CR1-mediated dendritic cell access to the intestinal lumen and bacterial clearance. Science. 2005; 307(5707): 254–258. [PubMed: 15653504]
24. Watchmaker PB, Lahl K, Lee M, Baumjohann D, Morton J, Kim SJ, et al. Comparative transcriptional and functional profiling defines conserved programs of intestinal DC differentiation in humans and mice. Nat Immunol. 2014; 15(1):98–108. [PubMed: 24292363]
25. Miller JC, Brown BD, Shay T, Gautier EL, Jojic V, Cohain A, et al. Deciphering the transcriptional network of the dendritic cell lineage. Nat Immunol. 2012; 13(9):888–899. [PubMed: 22797772]
26. Vander Lugt B, Khan AA, Hackney JA, Agrawal S, Lesch J, Zhou M, et al. Transcriptional programming of dendritic cells for enhanced MHC class II antigen presentation. Nat Immunol. 2014; 15(2):161–167. [PubMed: 24362890]

27. Aliberti J, Schulz O, Pennington DJ, Tsujimura H, Reis e Sousa C, Ozato K, et al. Essential role for ICSBP in the in vivo development of murine CD8alpha + dendritic cells. Blood. 2003; 101(1): 305–310. [PubMed: 12393690]
28. Schiavoni G, Mattei F, Sestili P, Borghi P, Venditti M, Morse HC 3rd, et al. ICSBP is essential for the development of mouse type I interferon-producing cells and for the generation and activation of CD8alpha(+) dendritic cells. J Exp Med. 2002; 196(11):1415–1425. [PubMed: 12461077]
29. Edelson BT, Kc W, Juang R, Kohyama M, Benoit LA, Klekotka PA, et al. Peripheral CD103+ dendritic cells form a unified subset developmentally related to CD8alpha+ conventional dendritic cells. J Exp Med. 2010; 207(4):823–836. [PubMed: 20351058]
30. Hildner K, Edelson BT, Purtha WE, Diamond M, Matsushita H, Kohyama M, et al. Batf3 deficiency reveals a critical role for CD8alpha+ dendritic cells in cytotoxic T cell immunity. Science. 2008; 322(5904):1097–1100. [PubMed: 19008445]
31. Holtschke T, Lohler J, Kanno Y, Fehr T, Giese N, Rosenbauer F, et al. Immunodeficiency and chronic myelogenous leukemia-like syndrome in mice with a targeted mutation of the ICSBP gene. Cell. 1996; 87(2):307–317. [PubMed: 8861914]
32. Rivollier A, He J, Kole A, Valatas V, Kelsall BL. Inflammation switches the differentiation program of Ly6Chi monocytes from antiinflammatory macrophages to inflammatory dendritic cells in the colon. J Exp Med. 2012; 209(1):139–155. [PubMed: 22231304]
33. Schraml BU, van Blijswijk J, Zelenay S, Whitney PG, Filby A, Acton SE, et al. Genetic tracing via DNGR-1 expression history defines dendritic cells as a hematopoietic lineage. Cell. 2013; 154(4): 843–858. [PubMed: 23953115]
34. Loschko J, Schreiber HA, Rieke G, Esterhazy D, Meredith MM, Pedicord V, et al. Absence of MHC class II on cDCs results in microbial-dependent intestinal inflammation. J Exp Med. 2016 in press.
35. Feng J, Wang H, Shin DM, Masiuk M, Qi CF, Morse HC 3rd. IFN regulatory factor 8 restricts the size of the marginal zone and follicular B cell pools. J Immunol. 2011; 186(3):1458–1466. [PubMed: 21178004]
36. Cassani B, Villablanca EJ, Quintana FJ, Love PE, Lacy-Hulbert A, Blaner WS, et al. Gut-tropic T cells that express integrin alpha4beta7 and CCR9 are required for induction of oral immune tolerance in mice. Gastroenterology. 2011; 141(6):2109–2118. [PubMed: 21925467]
37. Goubier A, Dubois B, Gheit H, Joubert G, Villard-Truc F, Asselin-Paturel C, et al. Plasmacytoid dendritic cells mediate oral tolerance. Immunity. 2008; 29(3):464–475. [PubMed: 18789731]
38. Darrasse-Jeze G, Deroubaix S, Mouquet H, Victora GD, Eisenreich T, Yao KH, et al. Feedback control of regulatory T cell homeostasis by dendritic cells in vivo. J Exp Med. 2009; 206(9):1853–1862. [PubMed: 19667061]
39. Kinnebrew MA, Buffie CG, Diehl GE, Zenewicz LA, Leiner I, Hohl TM, et al. Interleukin 23 production by intestinal CD103(+)CD11b(+) dendritic cells in response to bacterial flagellin enhances mucosal innate immune defense. Immunity. 2012; 36(2):276–287. [PubMed: 22306017]
40. Zigmond E, Bernshtein B, Friedlander G, Walker CR, Yona S, Kim KW, et al. Macrophage-restricted interleukin-10 receptor deficiency, but not IL-10 deficiency, causes severe spontaneous colitis. Immunity. 2014; 40(5):720–733. [PubMed: 24792913]
41. Cerovic V, Houston SA, Scott CL, Aumeunier A, Yrlid U, Mowat AM, et al. Intestinal CD103(−) dendritic cells migrate in lymph and prime effector T cells. Mucosal immunology. 2013; 6(1):104–113. [PubMed: 22718260]
42. Scott CL, Bain CC, Wright PB, Sichien D, Kotarsky K, Persson EK, et al. CCR2(+)CD103(−) intestinal dendritic cells develop from DC-committed precursors and induce interleukin-17 production by T cells. Mucosal immunology. 2015; 8(2):327–339. [PubMed: 25138666]
43. Tamura T, Tailor P, Yamaoka K, Kong HJ, Tsujimura H, O'Shea JJ, et al. IFN regulatory factor-4 and -8 govern dendritic cell subset development and their functional diversity. J Immunol. 2005; 174(5):2573–2581. [PubMed: 15728463]
44. Yamamoto M, Kato T, Hotta C, Nishiyama A, Kurotaki D, Yoshinari M, et al. Shared and distinct functions of the transcription factors IRF4 and IRF8 in myeloid cell development. PloS one. 2011; 6(10):e25812. [PubMed: 22003407]

45. Suzuki S, Honma K, Matsuyama T, Suzuki K, Toriyama K, Akitoyo I, et al. Critical roles of interferon regulatory factor 4 in CD11bhighCD8alpha -dendritic cell development. Proceedings of the National Academy of Sciences of the United States of America. 2004; 101(24):8981–8986. [PubMed: 15184678]

46. Lewis KL, Caton ML, Bogunovic M, Greter M, Grajkowska LT, Ng D, et al. Notch2 receptor signaling controls functional differentiation of dendritic cells in the spleen and intestine. Immunity. 2011; 35(5):780–791. [PubMed: 22018469]

47. Persson EK, Uronen-Hansson H, Semmrich M, Rivollier A, Hagerbrand K, Marsal J, et al. IRF4 transcription-factor-dependent CD103(+)CD11b(+) dendritic cells drive mucosal T helper 17 cell differentiation. Immunity. 2013; 38(5):958–969. [PubMed: 23664832]

48. Satpathy AT, Briseno CG, Lee JS, Ng D, Manieri NA, Kc W, et al. Notch2-dependent classical dendritic cells orchestrate intestinal immunity to attaching-and-effacing bacterial pathogens. Nat Immunol. 2013; 14(9):937–948. [PubMed: 23913046]

49. Tussiwand R, Everts B, Grajales-Reyes GE, Kretzer NM, Iwata A, Bagaitkar J, et al. Klf4 expression in conventional dendritic cells is required for T helper 2 cell responses. Immunity. 2015; 42(5):916–928. [PubMed: 25992862]

50. Wang Y, Ghoshal S, Ward M, de Villiers W, Woodward J, Eckhardt E. Chylomicrons promote intestinal absorption and systemic dissemination of dietary antigen (ovalbumin) in mice. PloS one. 2009; 4(12):e8442. [PubMed: 20041190]

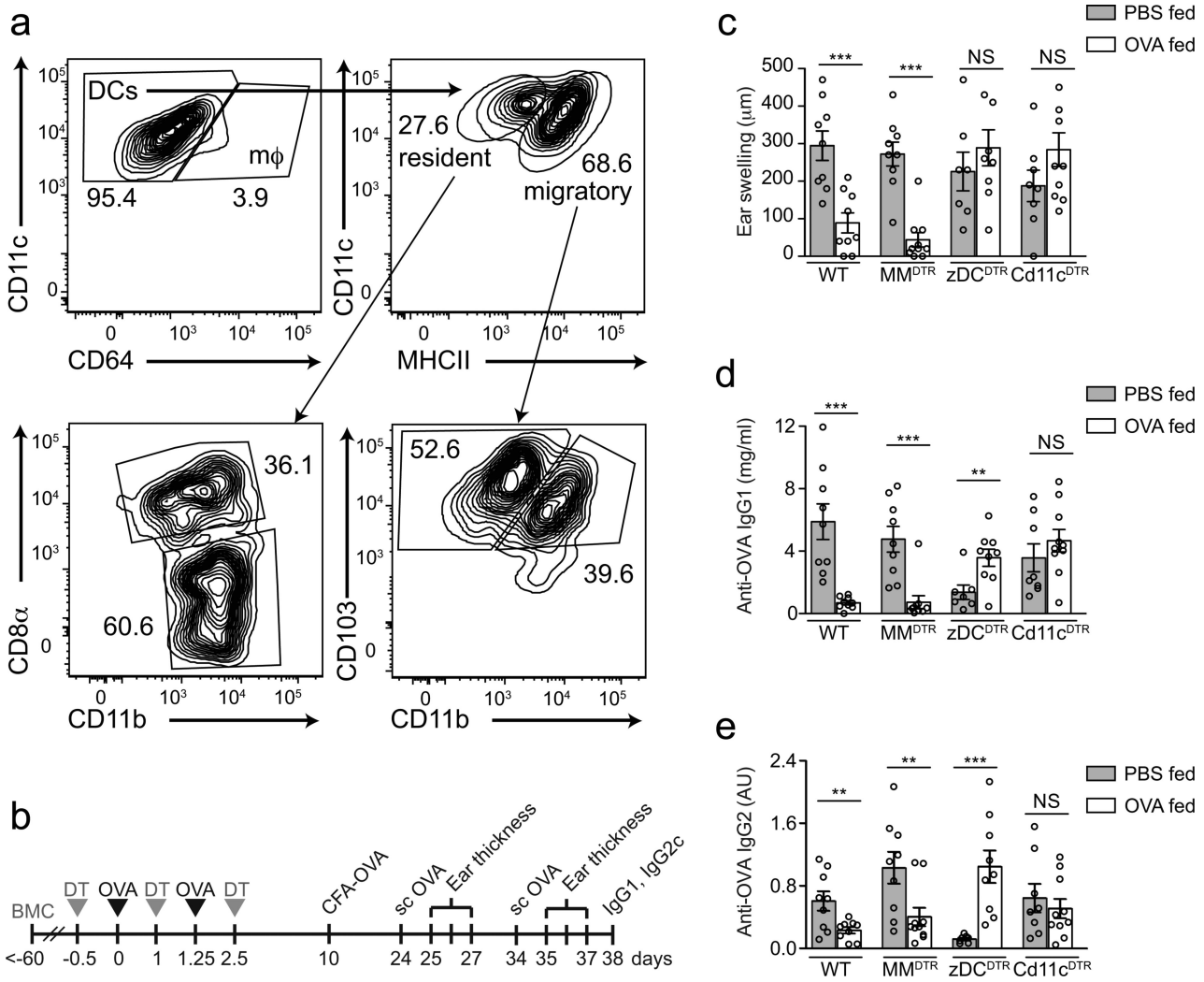

Figure 1. DTH responses in mice depleted of APC subsets during antigen feeding

(**a**) Flow cytometry contour plots of mLN macrophages and cDC subpopulations. (**b**) Experimental design of oral tolerance establishment towards CFA-mediated immunity. (**c**) Degree of ear swelling 48 h post second subcutaneous OVA challenge in wild-type, MM^{DTR}, zDC^{DTR} and $CD11c^{DTR}$ BMCs treated with DT during oral OVA (+) or PBS (−) exposure. (**d**) Serum anti-OVA IgG1 and (**e**) anti-OVA IgG2c levels in mice described in (c) 28 days post CFA immunization. Data represent pooled values (average±SEM) from two independent experiments, n=10 per group, ns= not significant, NS= not significant, *P<0.05, **P<0.01, ***P<0.005 (two-tailed t-test).

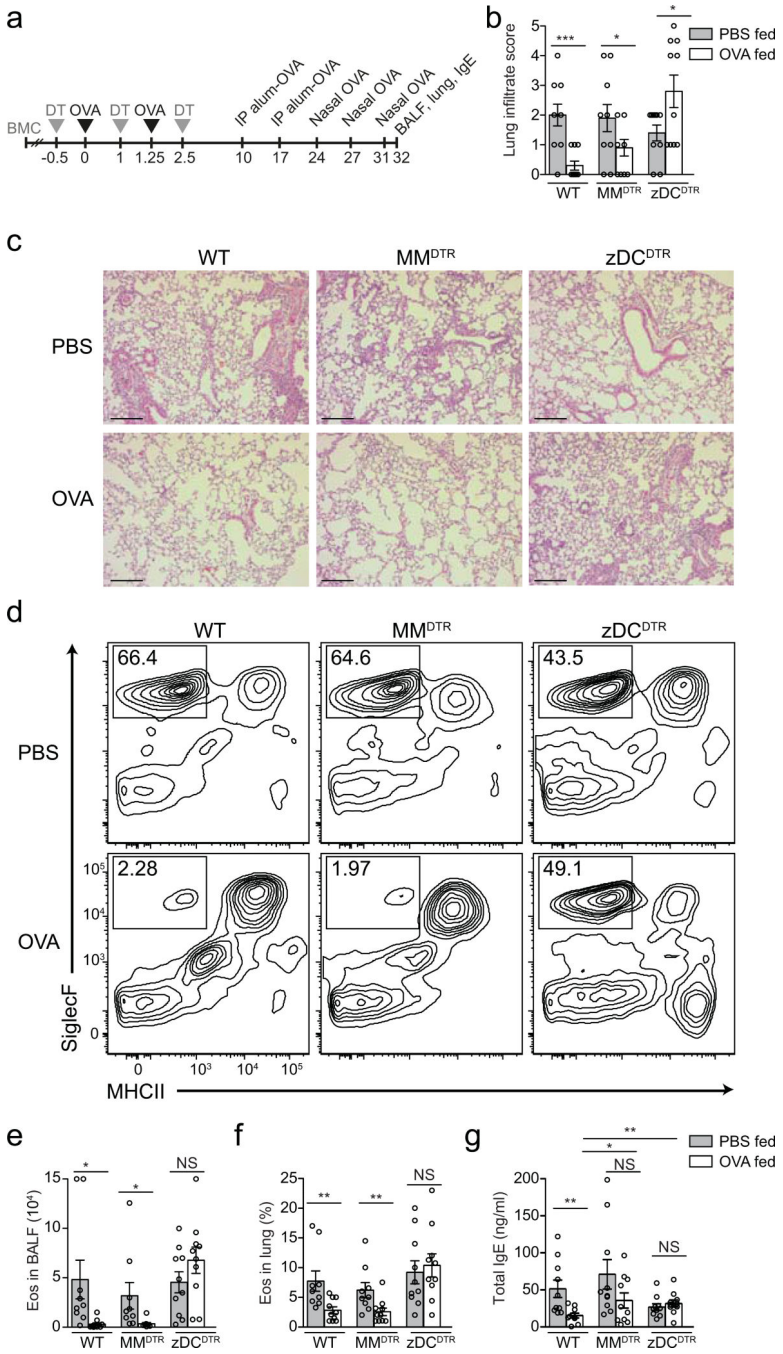

Figure 2. Allergic airway responses in mice depleted of APC subsets during antigen feeding

(**a**) Experimental design of oral tolerance establishment towards Alum-mediated immunity. (**b**) Histological score for inflammatory infiltrate and (**c**) representative hematoxylineosin staining of lung tissue from naïve (upper row) and OVA-gavaged (lower row) wild-type, MM^{DTR} and zDC^{DTR} mice. Scale bar, 250 μm. (**d**) Representative flow cytometry contour plot for $SiglecF^{+}MHCII^{-}$ gating (eosinophils, eos) in the BALF, and (**e**) analysis of total BAL eosinophil counts and (**f**) relative lung tissue eosinophil frequencies among $CD45^{+}$ cells in wild-type, MM^{DTR} and zDC^{DTR} BMCs treated with DT during oral OVA (+) or PBS

(−) exposure. (**g**) Serum total IgE in mice described in (**b-e**) 21 days post Alum immunization. Data represent pooled values (average±SEM) from two independent experiments, n=10 per group, NS= not significant, **P*<0.05, ***P*<0.01, ****P*<0.005 (two-tailed t-test).

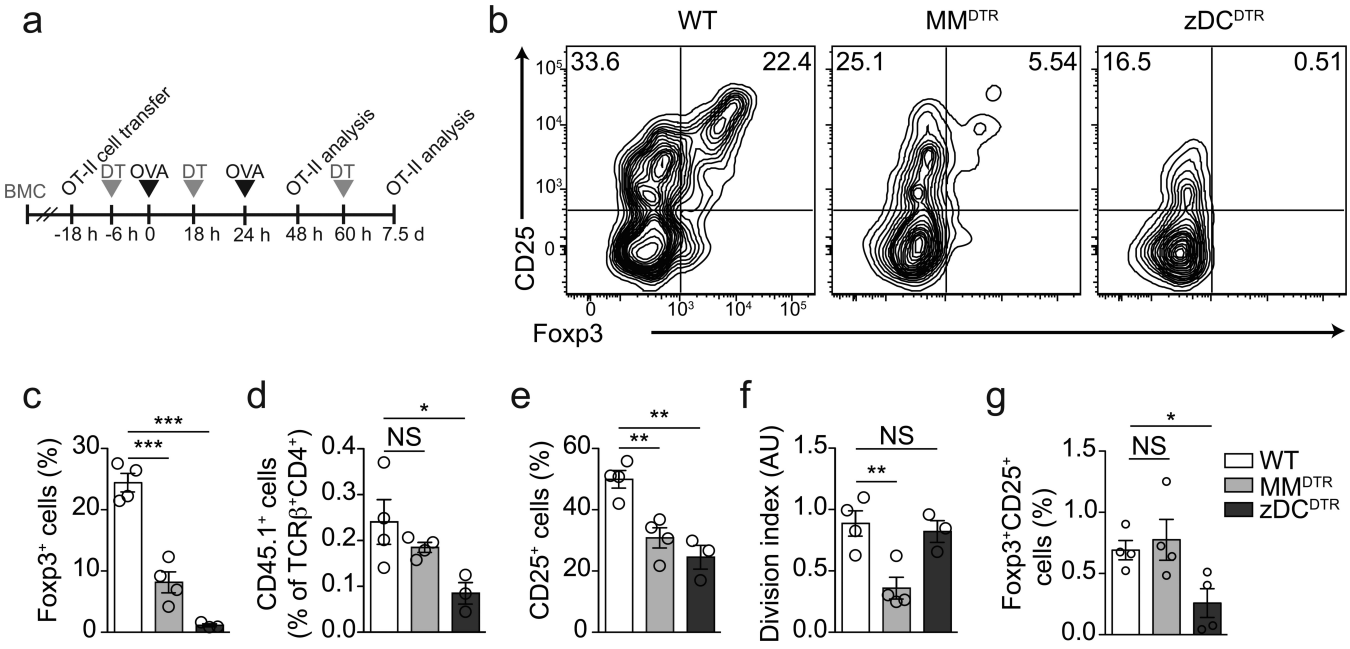

Figure 3. Contribution of macrophage-monocyte– and pre-DC–derived cells to pT_{reg} cell induction *in vivo*

(**a**) Schematic representation of *in vivo* pT_{reg} cell induction protocols. (**b-f**) Flow cytometry analysis of mLNs; (**b**) representative contour plots for Foxp3 and CD25 expression of $TCR\beta^+CD4^+CD45.1^+$ T cells; (**c**) $Foxp3^+$, (**d**) $CD45.1^+$, (**e**) $CD25^+$ cell frequencies and (**f**) cell division index of adoptively transferred naïve CD45.1 OT-II cells in the mesenteric lymph nodes (mLN) of wild-type, MM^{DTR} and zDC^{DTR} BMCs, 48 h after first oral OVA gavage. n=4. (**g**) Flow cytometry analysis of CD45.1 OT-II $Foxp3^+$ cell frequency in mLN of DT treated wild-type, MM^{DTR} and zDC^{DTR} BMCs, 7.5 days after first OVA gavage and 8 days post adoptive transfer of naïve CD45.1 OT-II cells. n=3. NS= not significant, *P<0.05, **P<0.01, ***P<0.005 (two-tailed t-test). Data (average±SEM) are representative of three independent experiments.

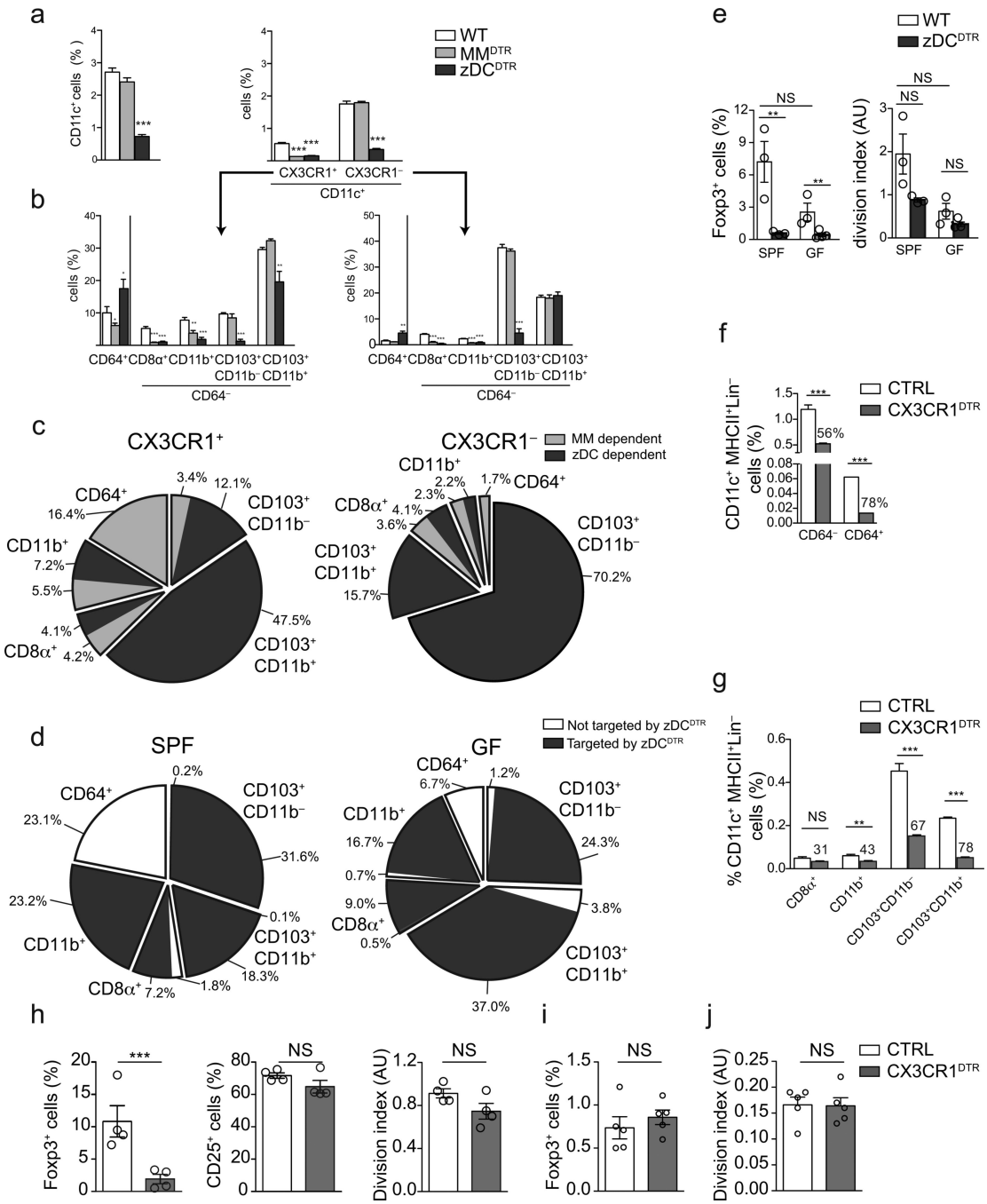

Figure 4. Contribution of CX3CR1^{+} cells to APC pools and pT$_{reg}$ cell induction

(**a**) Relative frequencies of CD11c^{+}, CD11c^{+}CX3CR1^{-} and CD11c^{+}CX3CR1^{+} among CD45^{+} cells, and APC subpopulations among (**b**) CX3CR1^{-} and CX3CR1^{+} (CD11c^{+}) cells in the mLNs of wild-type, MM^{DTR} and zDC^{DTR} BMCs, 36 h after DT administration. n=3. (**c**) Pie charts of relative MM (light grey) and cDC (dark grey) contributions to APC subpopulations within CX3CR1^{+} *versus* CX3CR1^{-} cell populations. n=4, ±SD. (**d**) Pie chart of flow cytometry analysis of APC subpopulations frequencies in the mLN within CD45^{+}Lin^{-}MHCII^{+}CD11c^{+} cells in SPF *versus* GF mice and targeting of the populations in

zDC^{DTR} mice (dark grey). n=4, ±SD. (**e**) Foxp3^{+} cell frequencies and cell division index of adoptively transferred naïve CD45.1 OT-II cells in the mLN of SPF *versus* GF, CX3CR1$^{GFP/+}$ *versus* zDC^{DTR} (CX3CR1$^{GFP/+}$) BMCs, 48 h after first oral OVA gavage. n=4 (**f, g**) Flow cytometry analysis of APC cell frequencies in the mLN of CX$_3$CR1$^{lsl\text{-}DTR}$ control *versus* CX3CR1^{DTR} BMCs, 36 h post DT administration. n=4. Numbers above CX3CR1 bars depict percentage reduction upon DT administration. (**h-j**) Foxp3^{+}, CD25^{+} cell frequencies and cell division index of adoptively transferred naïve CD45.1 OT-II cells in the mLN of CX3CR1$^{LsL\text{-}DTR}$ control *versus* CX3CR1^{DTR} BMCs, 48 h (**h**) or 7.5 days (**i, j**) after first oral OVA gavage. n=4, NS= not significant, **P*<0.05, ***P*<0.01, ****P*<0.005 (two-tailed t-test). Data (average±SEM) are representative of two independent experiments.

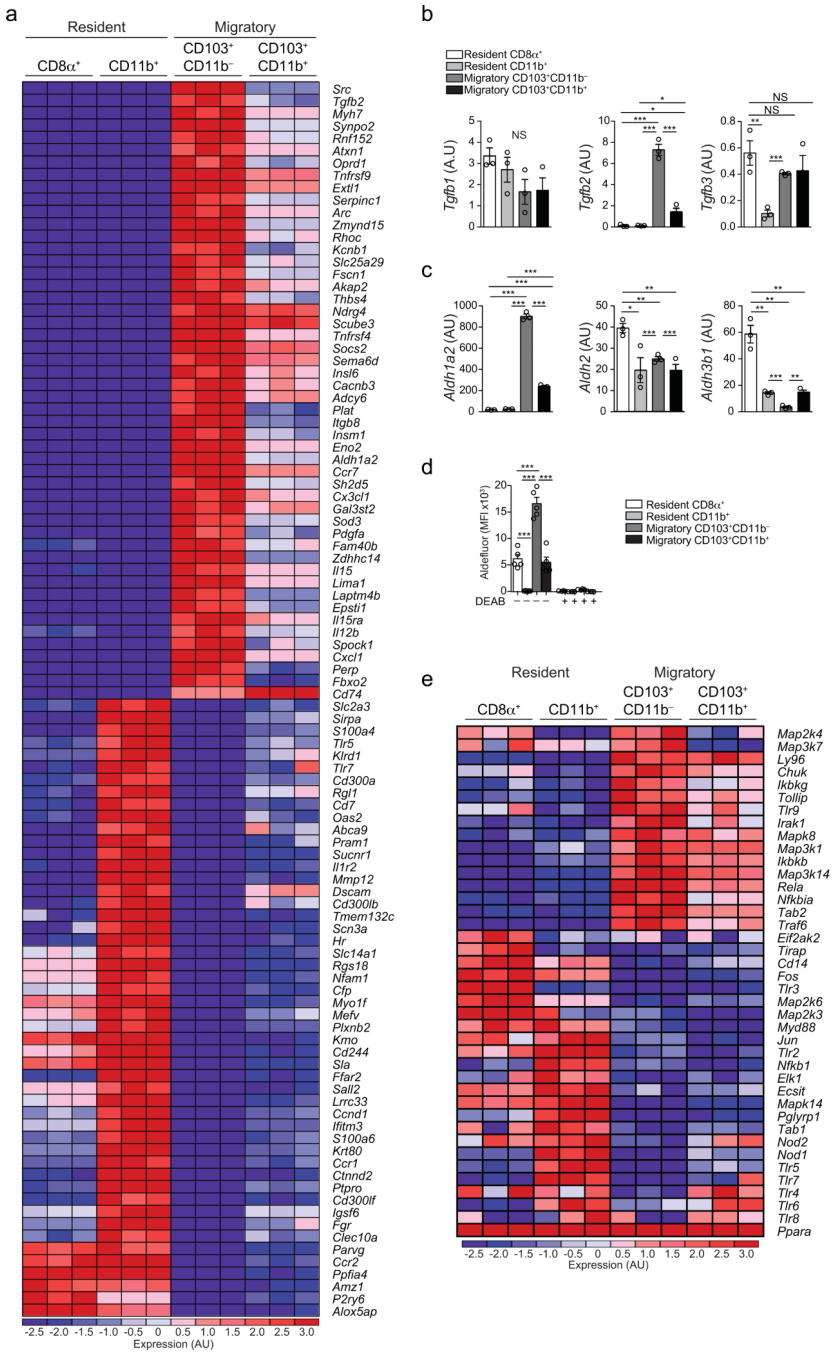

Figure 5. Characterization of mLN cDC subpopulations

(**a**) Heat map of most differentially expressed genes of cDC subsets in the mLN determined by RNA-seq. (**b**) Arbitrary units of TGF-β synthesis and (**c**) retinoic acid synthesis gene cluster expression levels in mLN cDC subsets determined by RNA-seq. (**a-c**) n=3, representing biological replicates. (**d**) Flow cytometry analysis of mean fluorescence intensity (MFI) of FITC^{+} Aldefluor conversion product in indicated mLN cDC populations after 30 min of substrate addition, pre-incubated with or without RALDH inhibitor DEAB. n=4 (biological replicates). Data are representative of four independent experiments. (**e**)

Heat map of expression levels of cDC subsets in the mLN determined by RNA-seq. n=3, as (**a**-**c**). Data shown as average±SEM; NS= not significant, **P*<0.05, ***P*<0.01, ****P*<0.005 (two-tailed t-test).

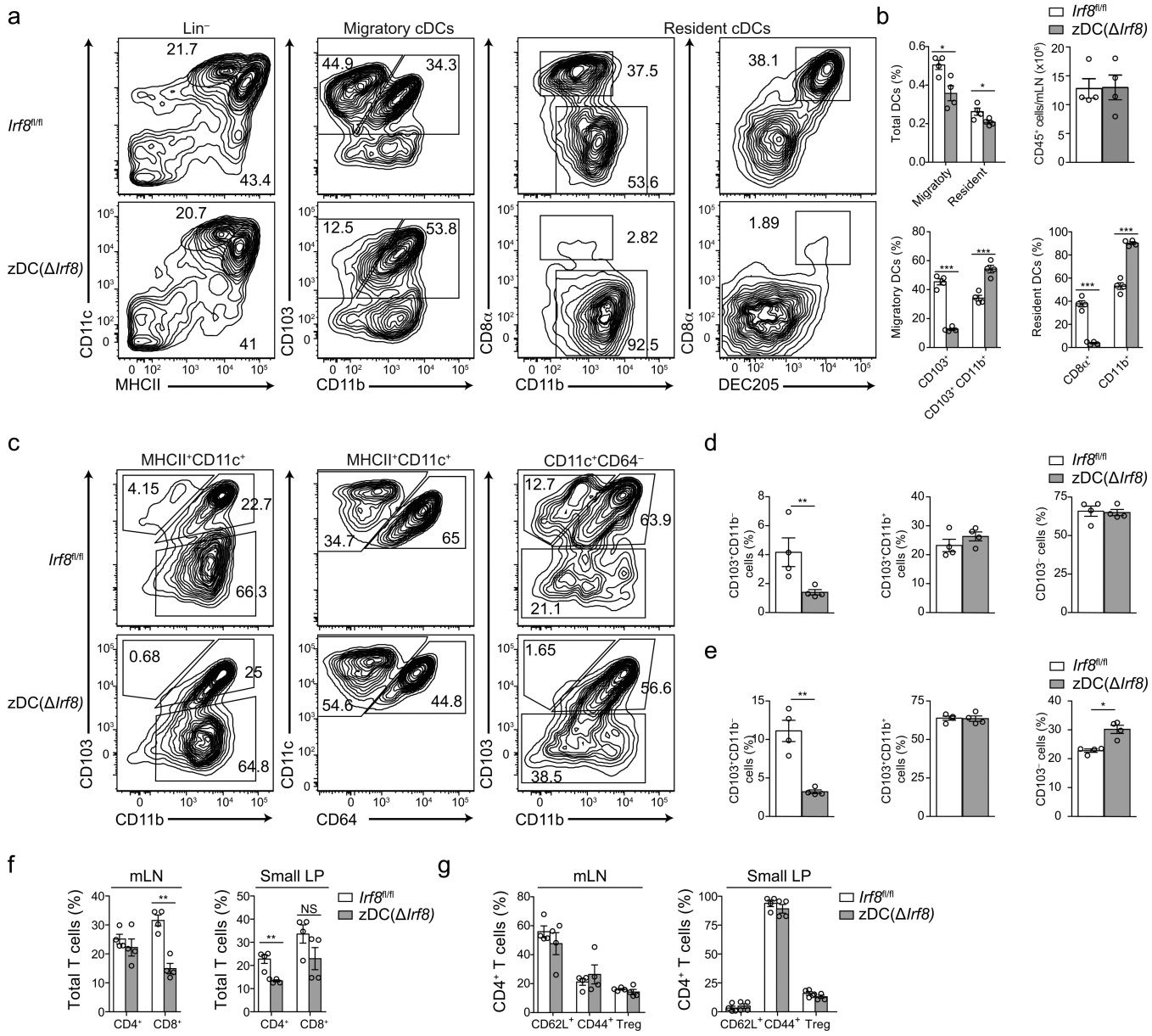

Figure 6. Analysis of steady state cDC and lymphocyte populations in the mLN and lamina propria of zDC(Δ*Irf8*) and *Irf8*$^{fl/fl}$ mice

(**a**) Representative flow cytometry contour plots, (**b**) relative frequencies of CD11c^{+}, CD11c^{+}MHCII^{hi} (migratory) and CD11c^{+}MHCII^{int} (resident) cDCs and total CD45^{+} cells in the mLN of *Irf8*$^{fl/fl}$ *versus* zDC(Δ*Irf8*) mice. (**c-e**) Representative flow cytometry contour plots (**c**) and relative frequencies among MHCII^{+}CD11c^{+} cells (**d**) or CD11c^{+}CD64^{-} cells (**e**) of small intestine *lamina propria* (LP) CD103^{+}, CD103^{+}CD11b^{+} and CD103^{-} DCs in 10 weeks old *Irf8*$^{fl/fl}$ *versus* zDC(Δ*Irf8*) mice. (**f**) mLN and small LP CD3^{+}CD8^{+} and CD3^{+}CD4^{+} cells, (**f**) mLN and small LP CD3^{+}CD4^{+}Foxp3^{+}, CD3^{+}CD4^{+}CD62L^{+} and CD3^{+}CD4^{+}CD44^{+} cells in 10 weeks old *Irf8*$^{fl/fl}$ *versus* zDC(Δ*Irf8*) mice. n=4, NS= not significant, **P*<0.05, ***P*<0.01, ****P*<0.005 (two-tailed t-test). Data (average±SEM) are representative of two independent experiments.

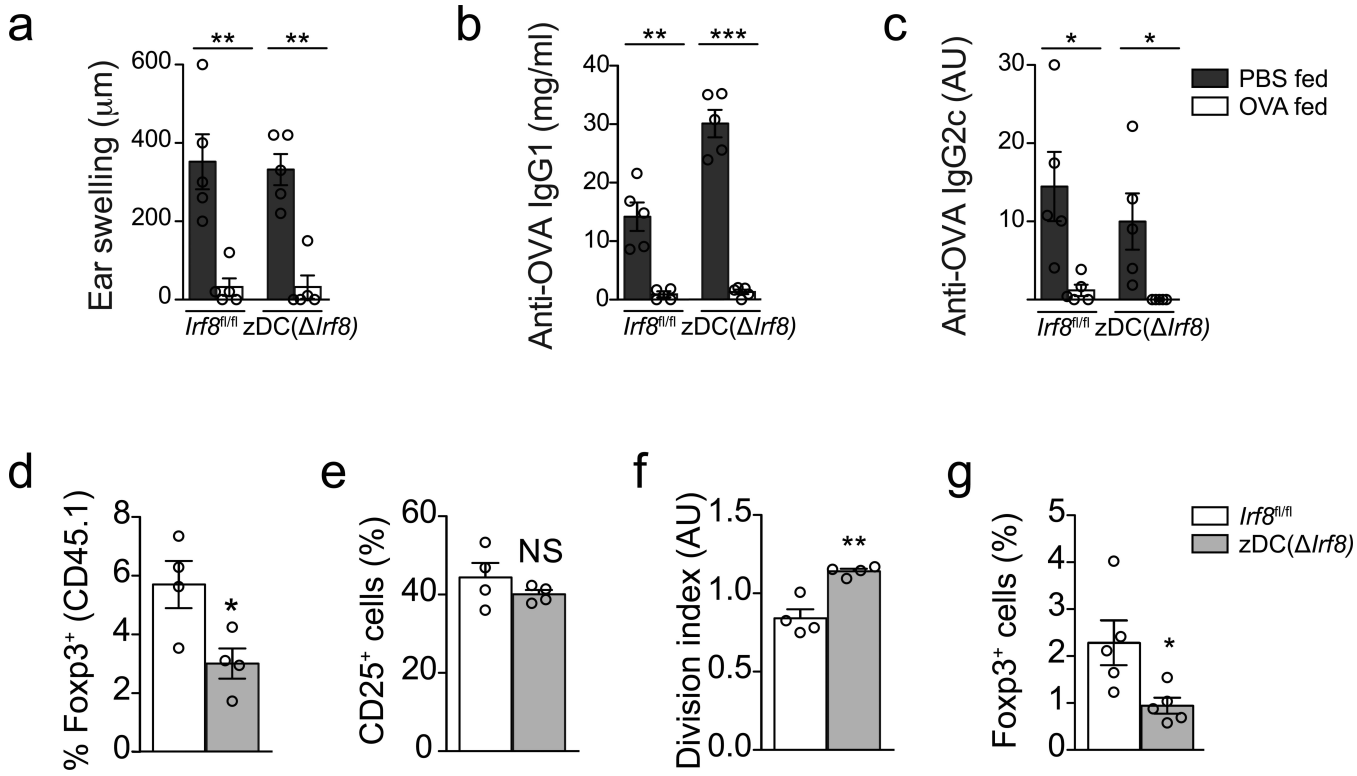

Figure 7. Assessment of oral tolerance and pT_{reg} cell induction in zDC(Δ*Irf8*) and *Irf8*$^{fl/fl}$ BMCs

(**a**) Degree of ear swelling 48 h post subcutaneous OVA challenge in *Irf8*$^{fl/fl}$ *versus* zDC(Δ*Irf8*) BMCs given oral OVA (+) or PBS (−) before immunization. (**b**) Serum anti-OVA IgG1 and (**c**) anti-OVA IgG2c levels in mice described in (**a**), 28 days post CFA immunization. n=5 per group. (**d-f**) Flow cytometry analysis of (**d**) Foxp3$^+$, (**e**) CD25$^+$ cell frequencies and (**f**) cell division index of adoptively transferred naïve CD45.1 OT-II cells in the mLN of *Irf8*$^{fl/fl}$ *versus* zDC(Δ*Irf8*) BMCs, 48 h after first oral OVA gavage. n=4. (**g**) Foxp3$^+$ cell frequencies of adoptively transferred naïve CD45.1 OT-II cells in the mLN of *Irf8*$^{fl/fl}$ versus zDC(Δ*Irf8*) BMCs, 7.5 days after first oral OVA gavage. n=4. Data (average ±SEM) are representative of two independent experiments each (a-c, d-f, g-h). NS= not significant, **P*<0.05, ***P*<0.01, ****P*<0.005 (two-tailed t-test).

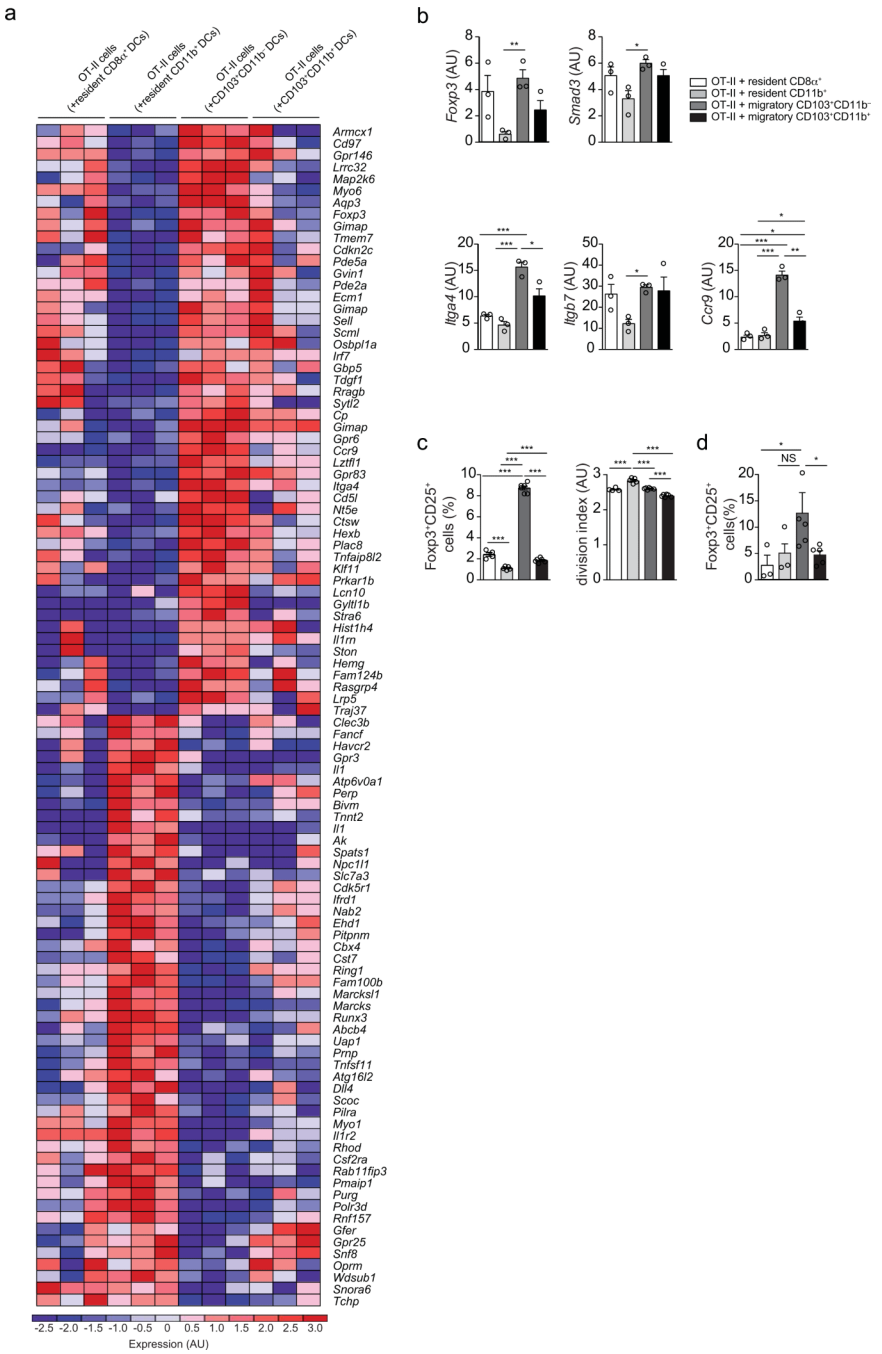

Figure 8. *In vitro* characterization of pT_{reg} cell induction potential of cDC subpopulations in the mLN

(**a**) Heat map of most differentially expressed genes in OT-II cells co-cultured with indicated mLN cDC subsets and OT-II peptide for 24 h determined by RNA-seq. n=3 (**b**) Treg and proliferation gene cluster expression levels of cDC subsets in the mLN determined by RNA-seq experiment shown in (**a**). n=3 (**c**) Flow cytometry analysis of $Foxp3^+$ frequency and cell division index of sorted naïve CD45.1 OT-II cells co-cultured with indicated mLN cDC subsets, OT-II peptide, anti-IL-4 and anti-IFN-γ antibodies for 72 h. n=4-6 (n=4 for resident and n=6 for migratory DC co-culture) from three independent DC donor pools. Data is

representative of three independent experiments. (**d**) Flow cytometry analysis of Foxp3^{+} frequency of sorted naïve CD45.1 OT-II cells co-cultured with indicated mLN cDC subsets obtained from mice that were fed an OVA-rich diet for 48 h, anti-IL-4 and anti-IFN-γ antibodies for 72 h. n=4-6 from three independent DC donor pools. Data shown as average ±SEM; NS= not significant, *P<0.05, **P<0.01, ***P<0.005 (two-tailed t-test).